Dynamic responses of reactive metallic structures under thermal and mechanical ignitions

Haoyan Wei and Choong-Shik Yoo[a)]
Department of Chemistry and Institute for Shock Physics, Washington State University, Pullman, Washington 99164-2816

(Received 30 May 2012; accepted 24 August 2012)

We have studied dynamic thermo-mechano-chemical responses of reactive metallic systems, both in clouds of small oxygen-free particles (~1–10 μm in diameter) produced by fracturing Zr-rich bulk metallic glass and in pure Zr metal foils (~25 μm thin), under thermal (laser ablation or pulse electrical heating) and mechanical loadings. The mechanical fracture/fragmentation and fragments reactions were time resolved using an integrated set of fast six-channel optical pyrometer, high-speed microphotographic camera, and time- and angle-resolved synchrotron x-ray diffraction. These small-scale tabletop real-time experiments performed on or near surfaces of reactive metals provide fundamental data, in atomistic scales or of particle clouds, regarding fragmentation mechanics, combustion mechanisms and kinetics, and dynamics of energy release under thermal and mechanical loadings. We present the results of pure Zr and Zr-rich amorphous metals, not only signifying diversified combustion mechanisms depending on microstructures, particle sizes, oxygen pressure, and ignition conditions but also providing fundamental data that can be used to develop and validate thermochemical and mechanochemical models for reactive materials.

I. INTRODUCTION

A new class of energetic materials emerges to reactive metals and metal alloys with advanced atomistic-to-nanometer scale microstructures such as bulk metallic glass and lamellae multilayers. Dynamic responses of these reactive bulk metals are fundamentally different from those of conventional reactive materials such as presynthesized metal particles, typically 10–100 μm in diameter, dispersed in explosives or reactive polymers. Characteristic to such novel reactive metals is the mechanical fracture, generating "fresh" oxygen-free small (sub- to a few micrometers) fragments on demand, which can readily burn at relatively low temperatures. This is unlike the way how larger metal particles with thin outside oxide layers would burn in conventional reactive materials, typically above melting temperatures of constituent metals. Importantly, small fragments of the reactive metals with high oxygen affinities such as Al, Zr, Ti, and Fe can immediately burn in air (or combust) and release a large amount of energy, making them of considerable interest to energetic materials research community.[1–3]

The combustion of these metals mainly involves two highly exothermic processes: primary metal combustion and secondary intermetallic reaction. Having produced a large surface area with fine metal fragments upon mechanical fracture, the reaction between metal particles and air (oxygen) can produce enough heat to rapidly reach very high temperature up to several thousand degrees, leading to the primary metal combustion in the early stage of combustion—likely the most energetic process of all governing reactions in reactive metal alloys. On the other hand, the secondary reactions such as the intermetallic reaction among metal constituents and the reactions of intermediates and products occur relatively slowly, because of large diffusion barriers between the grains of solid particles, and, thereby, dictate the reactions at later stages.

The total energy release of these reactions is often evaluated theoretically based on the thermodynamic properties of the associated chemical species such as internal energy, enthalpy, and heat of combustion.[4] Yet, the governing kinetics on the process of how the energy is released strongly depends on many specific materials properties and external conditions including particle size,[5,6] surface states, ignition approaches,[7] as well as oxidizing gas environment.[8,9] The rate and the extent of the combustion reaction, e.g., are directly linked to the fragment size. Relatively, small fragments of a few micrometers can be burnt nearly completely within very short reaction time (<1 ms). Yet, the reactions of larger particles (say 10–100 μm) with surrounding gases are typically limited to a very thin layer (less than a few micrometers)—forming huge gas diffusion and reaction barriers and, thus, leaving a significant portion of the large fragments unreacted and taking a substantially longer reaction time.

[a)]Address all correspondence to this author.
e-mail: csyoo@wsu.edu
This paper has been selected as an Invited Feature Paper.
DOI: 10.1557/jmr.2012.302

 © Materials Research Society 2012

https://doi.org/10.1557/jmr.2012.302 Published online by Cambridge University Press

The early stage of combustion mechanism (i.e., ignition) strongly depends on the surface condition of metal particles. For example, the presence of thin oxide layers on the surface of micrometer-sized metal particles limits the diffusion of oxygen and thus the combustion in solid metals. As a result, the combustion occurs typically from molten phases of metals above the melting temperatures.[10–12] The sudden expansion in volume of molten metal particles causes microcracks on metal oxide layers or even electric charges on metal particles, lowering the oxygen diffusion barrier. In contrast, small oxygen-free metal particles (sub- to a few micrometers in diameter) can ignite at relatively low temperatures well below the melting temperatures of metals.[13] Therefore, to understand these processes, it is critical to obtain in situ information regarding the exact dynamic nature of metal fragmentation and combustion such as the particle size, temperature evolution, and burn rates, as well as the reaction mechanism and kinetics of governing chemical reactions.

Microstructures, phase transitions, and defects on metal particles can greatly alter the mass (atomistic) and heat (thermal) diffusion processes and thereby influence chemical mechanisms and kinetics of metal combustion.[14–16] The presence of solid–solid or solid–liquid phase transitions, e.g., has a dramatic effect on the ignition process and combustion kinetics, which can lead to a microexplosion or an interesting "spear point" formation of oxide products.[14] Yet, a wide range of oxidation and intermetallic states viable in these reactive metals can give rise to an array of different oxides and intermetallic compounds depending on temperatures and reactant concentrations and, thereby, greatly complicate the reaction pathways. Furthermore, the dynamic (or transient) nature of combustions may result in the path-dependent phase and chemical changes and quenched metastable structures and secondary products. Therefore, obtaining time-resolved structural information during metal ignitions and combustions is critical to understand the chemical mechanisms, kinetics, and energetics. Such insights into details of reaction mechanism will provide the necessary information needed in the materials design to achieve tailored performance for diverse applications.

We previously reported size-dependent combustion kinetics of individual particles.[13] In this paper, we present our recent dynamic experimental results on bulk pure Zr and Zr-rich alloys, exhibiting strong dependences of Zr combustion on characteristics of metal fragments, microstructures, oxygen concentration, and ignition methods. These results were obtained using time-resolved optical pyrometry, microphotography, and synchrotron x-ray diffraction methods capable of probing thermal, chemical, and structural evolutions of metal fragments under short pulse laser ablation and small amplitude mechanical impacts.

The rest of the paper is organized as the following: In Sec. II, we describe the experimental methods; in Sec. III, we present the major findings regarding mechanical fragmentation, fragments combustion kinetics, and mechanism; in Sec. IV, we discuss about effects on combustion of fragment size, oxygen concentration, and thermal and mechanical ignitions; and finally, we make several concluding remarks in Sec. V.

II. EXPERIMENTAL METHODS

A. Short-pulse laser ablation and mechanical impact experiments

Metal particles of 1–100 μm diameters are the most studied objects in metal combustion because of their manufacturability and proper sizes in practical applications. Presynthesized powders are mostly used, which are covered with surface oxide layers. However, it has been shown that surface states could have a dramatic effect on the ignition behavior and subsequent combustion kinetics.[10,13] To produce particles with oxygen-free surfaces, a pulse microarc technique is utilized to electrically melt a tip of metal wire and form a molten droplet.[14,17] The particle diameter is typically restricted to 50 μm or larger in this methodology.

To complement the previous studies, we have developed an approach, which is able to generate small metal particles with fresh surfaces in the range of 1–10 μm in diameter. This method takes advantages of the ability of amorphous alloys to generate a sizable amount of small particles upon dynamic fracture because of their relatively brittle nature.

Figure 1 illustrates the device we use to produce small Zr-rich particles in the range of 1–10 μm. The particles can be created using two impulse methods: dynamic mechanical fracture and laser ablation. The dynamic mechanical fracture experiments were performed using a homebuilt compact impact device based on a ball bearing (BB) gun with projectile speed in the range of 20–100 m/s. The impact experiments were performed in a controlled gas

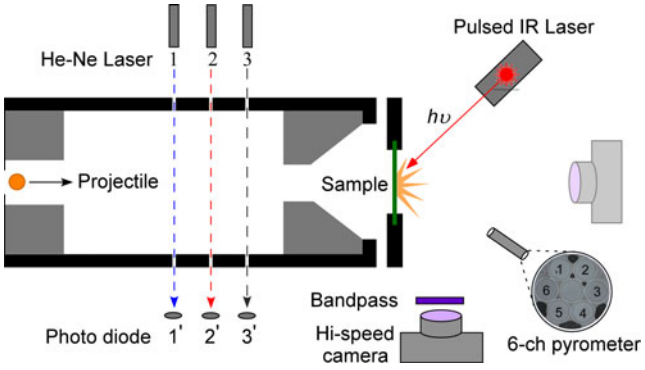


FIG. 1. The experimental setup for on-site particle generation and measurements of combustion kinetics. Small particles of 1–10 μm in diameter with fresh surfaces are created from bulk amorphous alloys by either mechanical impact (BB gun and a three-laser velocimeter) or laser ablation. Microphotography and photographic pyrometry based on a high-speed camera are utilized to investigate dynamic fracture and single particle kinetics. The global kinetics of particle cloud is investigated with a six-channel PMT-based pyrometer.

https://doi.org/10.1557/jmr.2012.302 Published online by Cambridge University Press

environment using synthetic air in an enclosed chamber, for both driving the BB gun and inducing the combustion. The impact velocity was determined using a three-position laser velocimeter. The fragmentation and combustion processes are recorded with a high-speed charged coupled device (CCD) camera (Photron FastCam SA-1, San Diego, CA) in either front view or side view position using a time resolution of 18/19 μs or smaller. Upon projectile impact on the sample, the bulk metal strips fracture, and the fine particles with freshly cleaved surfaces come out of the impact site and spread out into a conical plume. They then quickly react with oxygen leading to violent combustion. In contrast to the presynthesized particles with already oxidized surfaces, this approach generates particle on-site from bulk materials with completely oxygen-free surfaces. Such surface state would strongly influence the ignition behavior and thus combustion kinetics such as resulting in low ignition temperature.

Alternatively, we have produced a similar particle plume, thermally, by a laser ablation method. A pulsed CO_2 infrared (IR) laser is utilized to impinge the sample directly in either oblique or normal orientation. The highly concentrated energy nature in a very short time period instantaneously melts the ablation area, leading to the ejection of molten particles in a conical plume. Compared with the mechanical impact approach, laser ablation provides significantly higher input energy to heat the materials to melt states in a very short period.

B. Ultrafast multichannel optical pyrometry

The global temperature evolution is measured with a six-channel optical pyrometer constructed using photomultiplier tube (PMT) techniques. The principle of the pyrometer is based on Planck's radiation law as written in Eq. (1):

$$L(\lambda, T, \varepsilon) = \frac{\varepsilon C_1 \lambda^{-5}}{\exp\left(\frac{C_2}{\lambda T}\right) - 1} \quad , \qquad (1)$$

where the spectral radiance (L) is expressed as a function of wave length (λ), temperature (T), and emissivity (ε). Here, C_1 and C_2 are constants: $C_1 = 1.19108 \times 10^{-16}$ W m^2/sr and $C_2 = 1.4389362 \times 10^{-2}$ m K. The adoption of multiple channels eliminates the need for detailed emissivity value, which may not be always available. The pyrometer consists of three major components: light collection and transmission system (lens, mirrors, and optical fibers), photodetectors (PMTs), and signal processing units (digital oscilloscopes). As shown in Fig. 1, the light is collected and transmitted using 7-in-1 fiber bundles arranged in a hexagonal pattern. The extra center fiber bundle is used for alignment and future spectroscopy. The six discrete wave lengths are defined using bandpass filters with 10-nm full width half maximum in the range of 450–800 nm depending on the target temperature to be measured. The wave length spacing between adjacent channels is 50 nm or larger. Before measurements, the entire pyrometer system, including PMTs, fibers, filters, and other optics used, is calibrated against a blackbody radiation source. More detailed information about the pyrometer can be found in our other publications.[18,19]

C. Time- and angle-resolved synchrotron x-ray diffraction

Due to the large temperature range and multiple reactions in combustion, a variety of phase transformations can occur including melting, solidification, polymorphous transition, and oxidation. These processes have strong thermal activities (endothermic or exothermic), which would alter the energy flow in the reaction and thus have vast effects on the combustion kinetics. The fact that these processes can occur individually, in parallel, and/or interactively further complicates the analysis. The conventional method using reaction quenching and ex situ characterization is inadequate to probe the fast dynamic structural and chemical changes because quenching is unable to freeze the reactions. Instead, the thermal condition would be changed, leading to a different reaction pathway as demonstrated in the recent studies.[20,21] Therefore, a time-resolved structural and chemical probe with time resolution in the range of nanoseconds to microseconds is needed.

Recently, we have developed a novel time- and angle-resolved synchrotron x-ray diffraction (TARXD) technique to probe structural and chemical evolutions associated with metal combustions.[19] The system utilizes a fast rotating chopper to disperse the diffraction beam at different time onto different spatial regions of a two-dimensional (2D) x-ray detector (PILATUS, Dectris Ltd., Baden, Switzerland), as shown in Fig. 2. We used intense monochromatic synchrotron x-rays ($\lambda = 0.8638$ Å) from an undulator at the 16IDD (HPCAT) at the Advanced Photon Source (APS). The four-slot metal disk is placed in front of the detector, of which width and rotational speed determine the time resolution and the recording time of the detector. Zr foils

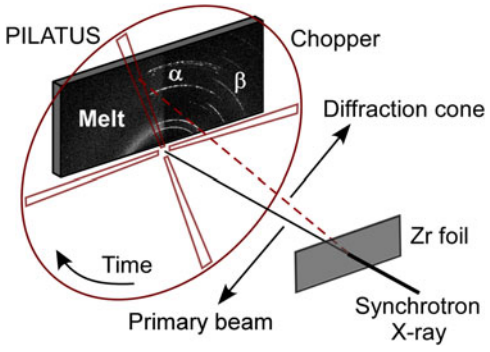


FIG. 2. A schematic drawing shows the experimental setup of TARXD to probe structural and chemical evolutions in metal combustion. The system uses intense monochromatic synchrotron x-rays, a 2D array detector (PILATUS), and a chopper based on a custom-designed slotted metal disk. As the chopper rotates, temporal diffraction patterns are dispersed spatially onto detector at different azimuth.

https://doi.org/10.1557/jmr.2012.302 Published online by Cambridge University Press

with active dimensions of 25 μm thickness, 150 μm width, and 300–500 μm length are used as samples and ignited by a pulsed electrical heating approach.[22]

The present TARXD method has several advantages over other time-resolved diffraction methods, which suffer from either a long readout time of the pixel array detector resulting in a relatively long blackout time (5–125 μs) between the frames or a poor spatial resolution of diffraction recorded on a small active area (15 × 13.8 mm^2, 100 × 92 pixels).[20,21,23] Moreover, only a limited number of successive frames (approximately eight) can be recorded in a row.[21] In contrast, the present TARXD method uses a substantially larger area detector (83.8 × 33.5 mm^2, 487 × 195 pixels)[19] to continuously record the diffraction images over a long period of time with relatively high time resolution. For example, at a time resolution of 45 μs, the total record period is about 3 ms over the entire detector area. This translates into about 60 consecutive diffraction patterns, providing the detailed information, without blackout time, of structural and chemical evolutions during the entire event of fast metal combustion. Furthermore, multiple diffraction images can be obtained using various kinetic modes of the detector, suitable for covering relatively slow reactions (over several 100 ms) such as intermetallic reactions and phase separation following the primary combustion.

III. RESULTS

A. Mechanical fracture and fragmentation

The reactive *bulk* metallic systems with atomistic-to-nanometer scale microstructures such as bulk metallic glass are of high strength yet very brittle without apparent slip systems. As a result, upon thermal or mechanical loadings, they can fracture and fragment, producing fresh small particles from the cracking surfaces. These fresh surface oxide-free small fragments are then immediately oxidized in air, which is a highly exothermic process [e.g., $Zr + O_2 \rightarrow ZrO_2 + \Delta H_f^0$ (−1100.6 kJ/mol)][24] as illustrated in Fig. 3.

Figure 3 shows two sets of high-speed camera frames (recorded at 54,000 fps) taken during two types of impact experiments on Zr-rich bulk metallic glass: (a)–(f) in air showing combustions of metal fragments and (g)–(l) in an inert gas (Ar) showing no chemical reaction. The samples were thin strips (16 × 6 × 0.5 mm) of Zr–Hf (atomic ratio 3:1, high purity >99.5%) amorphous alloys, made by an arc melting method. Similar to the latter experiment in Ar, no chemical reaction was observed in N_2, as well as in the experiments using "inert" metals including stainless steel foils (250 μm thick) or pure crystalline Zr foils (250 μm thick, 99.8%, annealed) impacted in air or nitrogen environment. The inert metal samples were only dented or bent, not fractured or shattered, even at the highest impact velocity of ~100 m/s applied in the present experiments.

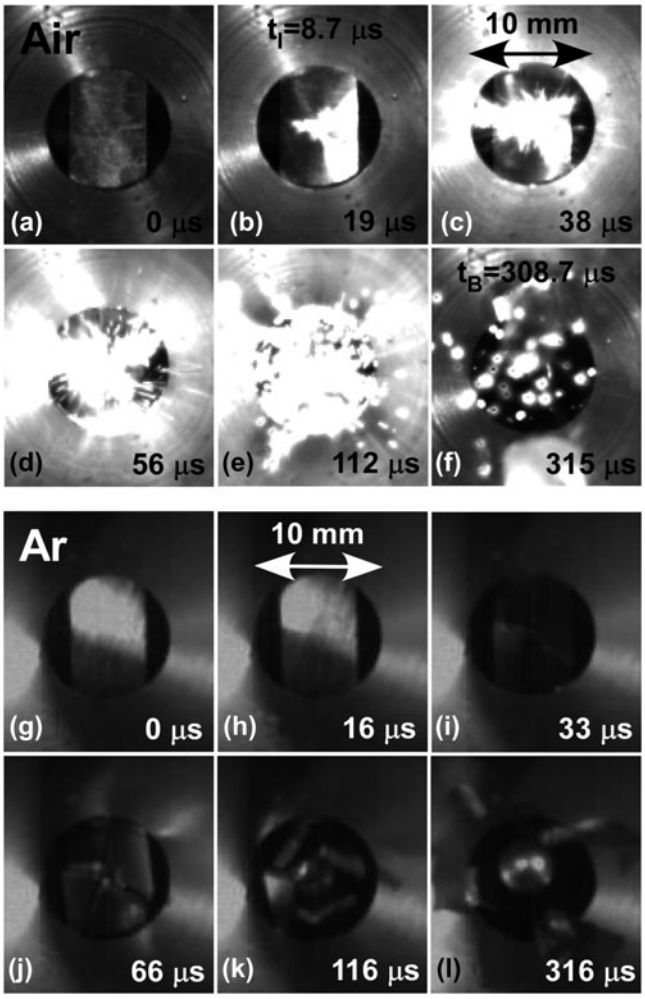


FIG. 3. The front views of high-speed optical imaging (a)–(f) show dynamic fracture of Zr-rich amorphous alloys and the intense light emission from their combustion in air. In contrast, no light emission or combustion is observed in inert atmosphere (Ar) under the same impact condition (g)–(l).

Figure 3(g)–(l) show that Zr-rich amorphous alloys in Ar can be shattered into small fragments, but no visible light emission is observed even under dark. Consistently, no light emission is detected by PMTs either. Our present pyrometer has a lower cutoff of about 1200 K due to limited wave length response of PMTs below 850 nm. The extended wave length response of CCD (up to ~1 μm)[13] should be to observe thermal radiance of metals above 700–800 K under dark. The absence of light recording thus indicates that the thermal contribution from impact-induced plastic deformation is not sufficient to heat the fragments (i.e., substantially lower than Zr melting point 2128 K), as expected from monolithic amorphous structures without any slip systems. This observation is consistent with previous measurements with IR detectors on bulk metallic glass in other research groups.[25–27] The intense light emission in Fig. 3(a)–(f), on the other hand, is clearly

https://doi.org/10.1557/jmr.2012.302 Published online by Cambridge University Press

from the rapid oxidization reaction, or combustion, of metal particles in air. In addition, the absence of visible light emission under N_2 implies that the metal nitridization and intermetallic reactions are either absent or do not produce sufficient heat leading to light emission in our alloys upon particle release.

The size of the particles produced is a key parameter in determining the exact nature of metal combustion such as burn time, burst temperature, and burn rate. We previously developed an aerodynamic drag model to characterize in-flight particle size through particle motion analysis.[13] To obtain the traveling path of burning particles, high-speed camera was placed normal to the project direction, recording the dynamic fracture in a side view as indicated in the experimental setup (Fig. 1). After recording, a series of recordings at different time stamps were superimposed together to obtain a composite image as shown in Fig. 4(a), which depicts the space–time trajectories of particles ejected from a metal strip upon a mechanical impact. The particles spread out in a conical shape as they are leaving away from the impact site. This makes it possible to resolve particles individually using the high-speed CCD camera both spatially and temporally. At every time stamp, two types of information can be obtained for each particle: the position and the light intensity. From the position information, we can obtain the particle displacement $s(x, y, t)$ in reference to the impact site [Fig. 4(b)]. x and y are particle coordinates at the time t. The displacement information of particles can be used to calculate the in-flight particle size based on the drag physics model.[13] Plotting Fig. 4(b) in a three-dimensional (3D) graph yields Fig. 4(c), where the z-axis (gray values) represents the light intensity. The total light intensity of a particle $I(x, y, t)$ is integrated gray value over the entire particle, which can be used to derive the single particle temperature based on the Planck's radiation law. Readers interested in this aspect can find the details in our previous publication.[13]

Figures 4(d)–4(f) show the particle size and velocity information as well as their correlation. To have statistical information, the analysis was done on a large number of

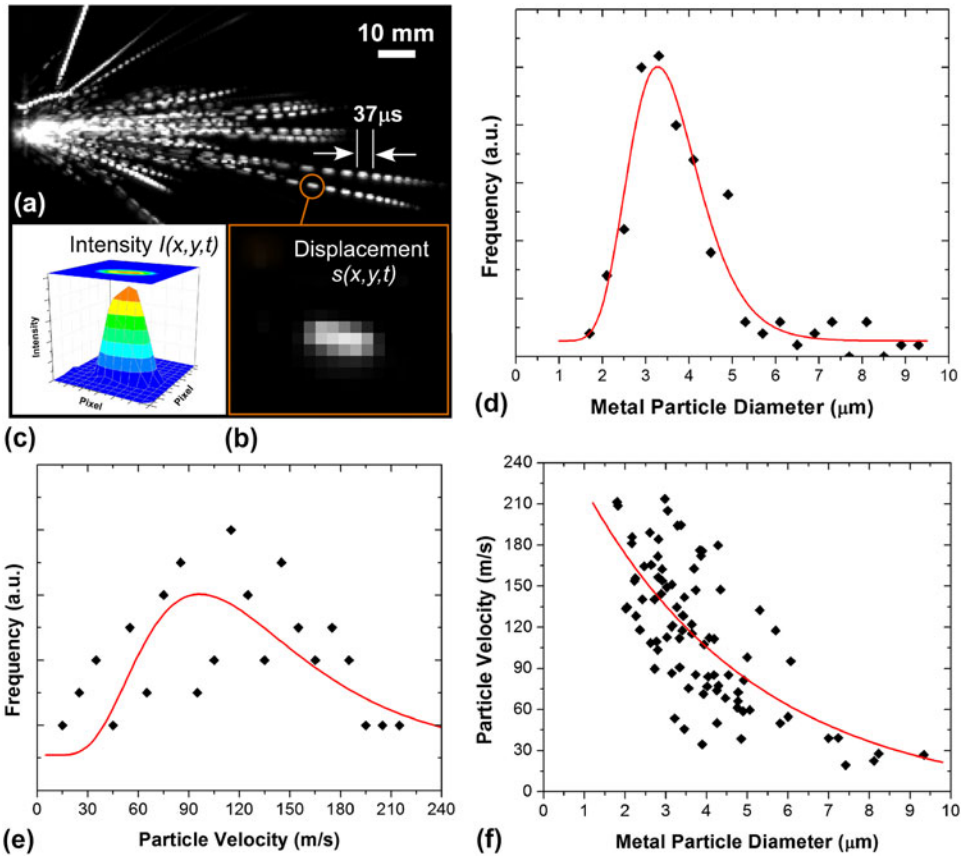


FIG. 4. (a) A superimposed image of every other high-speed camera records (at 54,000 fps or 18/19 μs time resolution), showing the spatial–temporal trajectory of burning particles ejected from a metal strip by mechanical impact. The particles fly out of the impact site (the left side) and spread into a plume toward right side. (b) and (c) illustrate the close-up view of a particle in 2D and 3D plots at a specific time, respectively. The displacement s and light intensity I of the particle can be measured as a function of coordinates (x, y) and time (t), from which particle size and temperature can be derived based on aerodynamics and Planck's law. (d), (e), and (f) Characteristics of metal fragments produced by mechanical impacts on Zr-rich bulk metallic glass: particle diameter, particle velocity, and correlation between particle size and velocity.

https://doi.org/10.1557/jmr.2012.302 Published online by Cambridge University Press

samples. The particle size and particle velocity were derived over a hundred of particles. Figure 4(d) indicates that the particles produced from Zr-rich bulk metallic glass by mechanical impact are in the range of 1–10 μm in diameter with the size distribution of a typical lognormal profile and a mode value of about 3.0–3.5 μm. Note that these small particles typically burn nearly completely and, thus, are critical in determining the energetics and impulse characteristics of combustion. Yet, the previous combustion experiments were mostly performed on larger particles (>20–50 μm) typically with thin oxide layers on metal surface.[28–30] The starting particle velocities range over 15–220 m/s approximately with a lognormal distribution, as illustrated in Fig. 4(e). The correlation between the particle size and velocity is also shown in Fig. 4(f), exhibiting an exponential decay. This is consistent with the momentum conservation law, where higher initial velocity is observed for smaller particles that have less mass.

B. Fragments combustions and global kinetics

Real-time temperature information is critical in evaluating chemical kinetics and energetics of reactive materials. For example, in an adiabatic approximation and an Arrhenius-type reaction rate, the combustion process can be described by a "global" kinetic model in terms of the combustion temperature, representing the energetics of *overall* chemical reactions, and the burn time, representing the reaction rate of *overall* chemical species, as illustrated in Fig. 5.

Figure 5(a) shows a typical time-resolved temperature profile of metal particles in combustion, measured using the six-channel optical pyrometer. The profile shows that, after a brief induction period at low temperature, the measured temperature rises initially rapidly to ~80–90% of the peak value, then slowly to the peak value for the next few 100 μs. Apparently, the rate of heat generation of exothermic reactions of metal particles surpasses the rate of combined heat dissipation through a conductive loss to the cold unreacted portion of metal particles, a convective loss to air, and a radiative loss, in this primary combustion period. After reaching the peak temperature, the temperature gradually decreases over the entire combustion period of 1–1.5 ms, representing gradual depletion of unreacted materials and cooling of metal oxides in this secondary combustion period.

To quantify the combustion process, we define several key parameters of the temperature profile as denoted in Fig. 5(a), including the instance of impact (t_0), initiation time (t_I), burst time (t_B), burst temperature (T_B), and burn rate. The instance of impact (t_0) is calculated using the measured impactor velocity and the distance between the first photodiode and sample (see Fig. 1). The initiation time (t_I) is when temperature starts to increase rapidly, and the induction period is then defined by ($t_I - t_0$). The burst time (t_B) is when the temperature reaches the peak value (defined as the burst temperature T_B). The burn period or time (Δt_c) and combustion period (or time) are then defined as ($t_B - t_I$) and the total light emission time, which depicts the primary (the most energetic process) and entire combustion

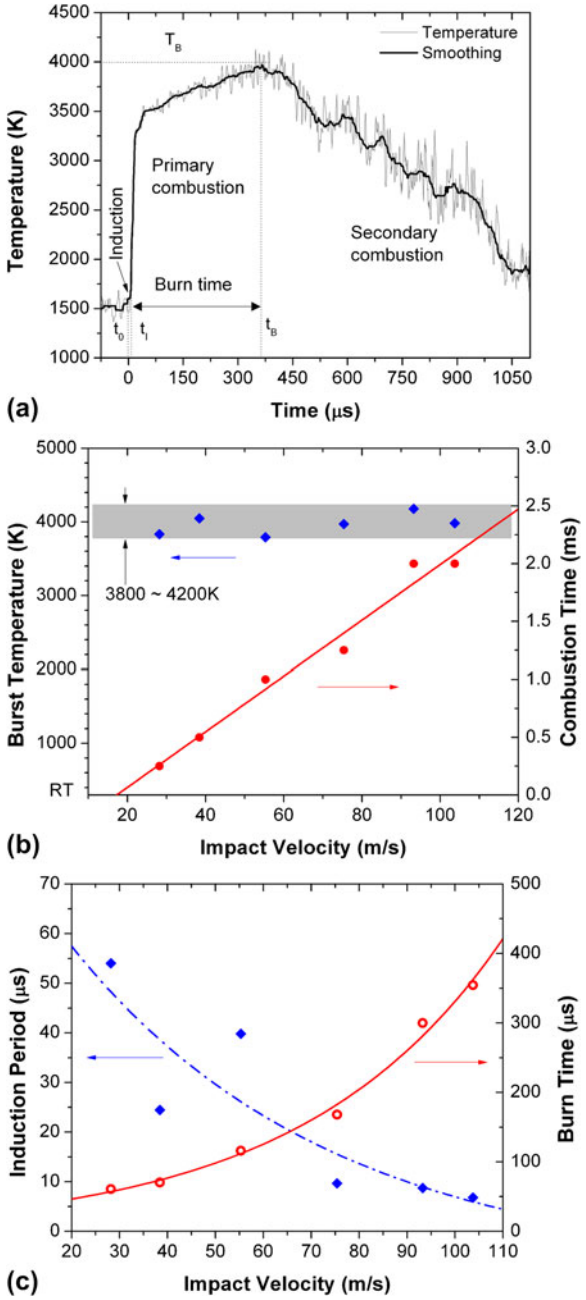


FIG. 5. (a) A global combustion model based on the temperature evolution of mechanically initiated combustion of Zr-rich amorphous alloys. Critical times (t_0, t_I, t_B, burn time) and temperature (T_B) are defined to quantify the combustion process. (b and c) The chemical performance data of Zr-rich amorphous alloys as a function of the impact velocity in a divergent geometry, signifying the reaction energetics (b) and global reaction kinetics (c) of metal combustion processes.

https://doi.org/10.1557/jmr.2012.302 Published online by Cambridge University Press

(including the cooling period) processes, respectively. Burn rate is then defined by the slope of the steep temperature rising edge at the initial stage.

Based on the above-described "global" combustion model, one can gain insight into chemical performance of Zr-rich bulk metallic glass under mechanical impacts, in terms of the energetics [T_B and combustion time in Fig. 5(b)] and kinetics [t_I and Δt_c in Fig. 5(c)] associated with the combustion process. The most striking result is that all measured burst temperatures are about ~4000 (±200) K, nearly independent from the impact velocity. This result likely reflects that we are measuring a single event reaction process of $Zr + O_2 \rightarrow ZrO_2$, e.g., which must have a characteristic combustion temperature under an adiabatic process. Consistently, this burst temperature of particle clouds measured globally is in excellent agreement with that of individual particles in 3.0–3.5 μm diameter [the most frequent size as shown in Fig. 4(d)] in our previous single particle measurements, which also exhibit a peak temperature of about 4000 K.[13] Equally important is the induction time that shows an exponential dependence with the impact velocity. It ranges from less than 10 μs at the maximum velocity of ~100 m/s to over 50 μs at the reaction threshold velocity of ~24 m/s. We also noticed a substantially large variation in the induction time, depending on the chemical composition.[31] Other interesting information is the burn and combustion periods, which represent the energy releases during the primary and overall combustion processes, respectively. Both the records show an increase with the impact velocity, consistent with the fact that a larger amount of particles are produced and burnt at a higher velocity. On the other hand, the different power dependences of these records are not well understood; those are the nonlinear dependence of the burn period and the linear dependence of the combustion period.

C. Combustion mechanisms

Over the large temperature range, metal combustion involves a variety of structural and chemical transitions including polymorphous, melting, solidification, and oxidation. As demonstrated in our study on single particle combustion,[13] a sudden temperature rebound or microflash in light intensity is present in the later stage of combustion, indicating exothermic liquid–solid and/or solid–solid phase transformations. As a result, chemical kinetics and reaction paths can be dramatically changed, leading to different final products.

For combustions in Zr-rich metal alloys, ZrO_2 is traditionally considered as the major product even under incomplete combustion based on the equilibrium phase diagram.[17,32] Previous studies using microstructural and compositional analysis seem to support that the ZrO_2 is precipitated out directly from the oxygen-saturated Zr–O solutions through a eutectic reaction ZrO_x ($x < 2$) → α-Zr + ZrO_2. However, considering a wide range of oxidation states viable in metals and the highly nonequilibrium environment in combustion can give rise to an array of different oxides depending on oxygen concentration and diffusivity; the exact reaction routes remain unclear with the static characterization techniques. Therefore, it is imperative to decipher the combustion mechanism with time-resolved structural and chemical information.

We have applied our fast rotating chopper-based TARXD to study the phase evolution of several transition metals in a previous publication.[22] Here, we briefly review the Zr results to understand the combustion mechanism and compare the reaction products in Zr-based alloys with different geometry and composition. Figure 6 shows the dynamic phase transformation and chemical oxidation of Zr foil combustion using time-resolved

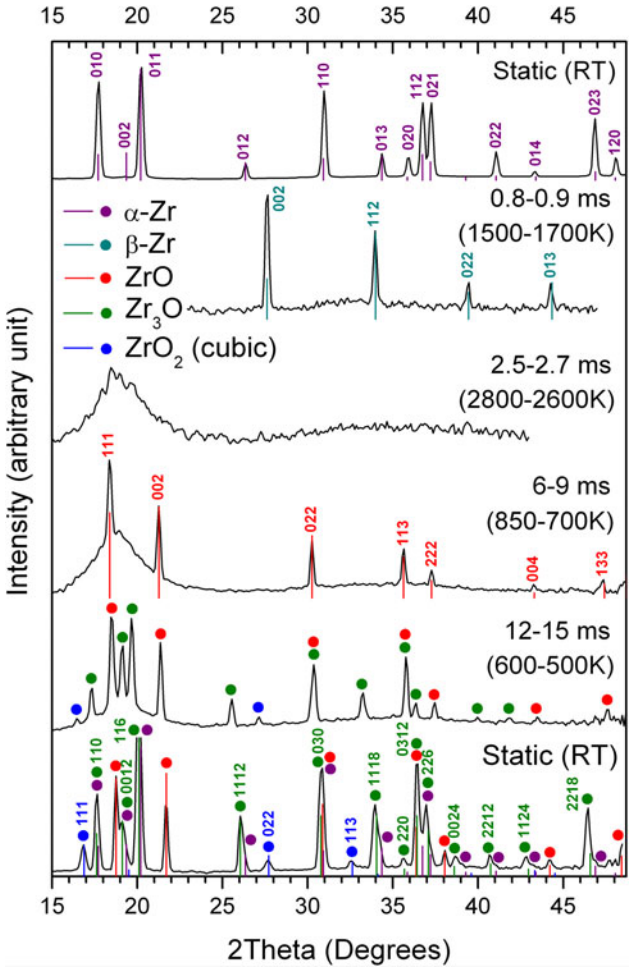


FIG. 6. Time-resolved powder x-ray diffraction patterns of Zr foils in combustion, obtained by integration of the TARXD images as illustrated in Fig. 3 over a discrete time period as noted in the figure. The simulated diffraction peaks are superimposed as marked by vertical color lines. The indices of each phase are also indicated. Reproduced from Ref. 22 and used with permission.

https://doi.org/10.1557/jmr.2012.302 Published online by Cambridge University Press

synchrotron diffraction technique with a time resolution of 45 μs. The pyrometer-measured temperature is also indicated in each diffraction patterns. The top diffraction represents the original *hcp* α-Zr. At ~0.8–0.9 ms after the ignition by electrical pulse heating, a new set of sharp diffraction lines (indicated by dark cyan) appears indicating the polymorphous transition of α-Zr into *bcc* β-Zr. The measured temperature is about 1500–1700 K above the phase transformation point (1136 K). Subsequently, β-Zr melts as the temperature increases above the melting point, apparent from the broad halo features in the measured x-ray diffraction patterns (the records from 2.5 to 15 ms). The corresponding temperature also indicates that it is above the Zr melting point (2128 K). As the temperature decreases after the peak point, high temperature metastable phase ZrO in *fcc* emerges as the first oxide product at about 6–9 ms, clearly from molten Zr (not solid). As the temperature continually decreases to about 600–500 K, additional diffraction features appear at ~12–15 ms, from two other forms of Zr oxides, cubic ZrO_2 and trigonal Zr_3O. At substantially later time when the reaction reaches the final state, residual α-Zr metals are also observed, in addition to the three Zr oxides mentioned above.

This observation highlights that a "simple" process like Zr combustion is barely the same as $Zr + O_2 \rightarrow ZrO_2$ as widely believed in previous studies using static or slow characterization techniques. The TARXD study clearly indicates that the combustion of Zr in air is a process strongly controlled by oxygen diffusion, which involves rather complex structural and chemical changes. These transitions are either exothermic or endothermic, which change the heat flow in the combustion thus greatly affecting kinetics. Understanding these dynamic processes is a challenging task and requires the development to the state-of-the-art time-resolved atomistic probes, but the potential payoff is enormous such as developing a predictive capability through more accurate chemical models and ultimately controlling the reaction routes, dynamics, and kinetics to meet different application requirements.

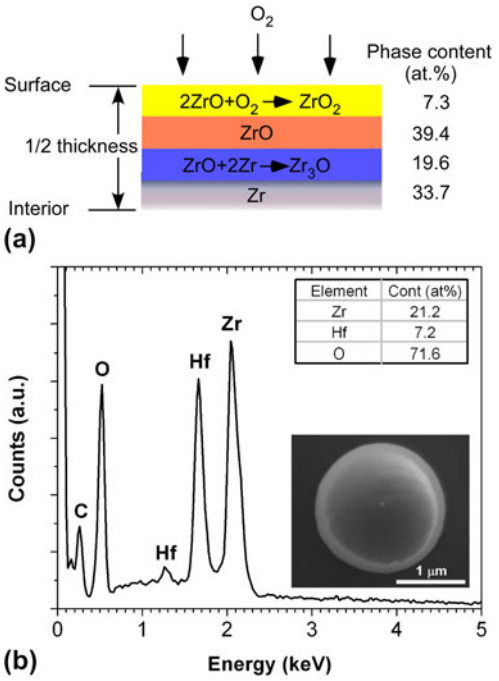


FIG. 7. (a) A model showing the combustion mechanism of Zr metals. The transition from higher oxides at exterior to lower oxides at interior indicates the reaction is an oxygen diffusion limited process. (b) The EDS spectrum implies that small Zr-rich particles are completely oxidized according to the higher ratio of oxygen to metal than that of stoichiometric dioxides. The inset SEM picture illustrates a representative burned particle of about 1.8 μm diameter. (b) is reproduced from Ref. 13 and used with permission.

IV. DISCUSSION

A. Combustion mechanism dependence on fragment structures

Oxygen diffusion is the most critical process governing metal combustions, which strongly depends on the microstructure, size, and shape of metal fragments. Based on the time-resolved x-ray diffraction study on 25-μm-thick Zr foil combustion, we propose a model to describe the oxidation process as shown in Fig. 7(a). Along the foil thickness direction or oxygen diffusion path, combustion products change from oxygen-rich phases to oxygen-deficient phases from the sample surface to the interior. The diffusion-controlled combustion process gives rise to multiple phases that are not present in the equilibrium phase diagrams or under equilibrium conditions. The initial oxide products are metastable ZrO, rather than more thermodynamically favored ZrO_2 at high pressures and temperatures. Note that ZrO is the most oxygen-deficient oxide available at high temperatures near the melt.

While oxygen continues to diffuse into the central area of the foil through the already formed oxide layers driven by a large concentration gradient, the coexistence of multiple phases creates a series of interfacial boundaries where an array of phase/chemical transformations can occur simultaneously. At the outer surface layer in contact with the air, ZrO reacts with oxygen to form the highest stoichiometric metal oxides ZrO_2. At the inner interface between monoxides and unreacted metals, their reaction leads to the formation of even lower suboxides Zr_3O at temperature around 700–500 K as observed in TARXD (Fig. 6), which is consistent with their presence at low temperature regime as indicated in the phase diagrams.[33–35] The stoichiometric composition of Zr_3O represents the upper solubility limit of oxygen ordering in α-Zr. At the innermost region, residual Zr metals are present.

Note that the above-described combustion mechanism of Zr foils producing a wide range of oxygen-deficient metal oxide products is in sharp contrast to those of

https://doi.org/10.1557/jmr.2012.302 Published online by Cambridge University Press

preformed metal particles of the previous studies[16,17] and of small fresh particles produced from Zr-rich bulk metallic glass in our study as described below [Fig. 7(b)].

The formation of oxide layers on the surface tends to limit oxygen diffusion and thus further combustion in solid metals. Yet, high thermal conductivity of unreacted metals rapidly dissipates the heat of combustion produced on the surface. As a result, the oxidation of larger metal particles (10–100 μm) is often limited to a very thin layer (less than a few micrometers). In our thin foil combustion experiments, we measured about 7–8 at.% ZrO_2 in the final products, which accounts for about 5–6 at.% of the total Zr consumed. This translates into a 1–2 μm thickness of Zr that is completely oxidized. This agrees well with the observed complete oxidation in the case of small particles (sub- to a few micrometers in diameter).

As shown in Fig. 7(b), a burnt particle of about 1.8 μm was recovered from the dynamic fracture of Zr-rich amorphous alloys. The composition analysis with energy-dispersive x-ray spectroscopy (EDS) indicates that oxygen to metal atomic ratio is about 2.5, higher than their highest oxides ZrO_2 and HfO_2. Considering that the excitation volume of EDS (about 1 μm) is slight larger than the radius of the particle shown, the EDS data should reflect a result of the entire particle (from the surface to the core) that has been oxidized symmetrically. This implies that the particle is completely oxidized. The comparison above reflects the delicate balance among fragment size and final combustion products with respect to diffusion length. On the other hand, the role of geometry may not be overlooked. The foils have much smaller dimension in thickness (25 μm) than width and length (150 and 300–500 μm, respectively). Therefore, the oxygen diffusion takes place primarily along the thickness direction. In contrast, oxygen diffusion can occur in all the radial directions in spherical particles, which could promote the diffusion activity.

Another important difference between the foils and particles in this study is the distinct ignition mechanism. As shown in Fig. 6, oxidation initiates only from molten metals in thin foil combustion. This is likely due to higher solubility of oxygen in molten metals and higher activation barrier for oxygen diffusion through solids because of the large fragment size and presence of surface oxides. This is consistent with the general ignition mechanism observed in presynthesized metal particles with larger diameters such as Al oxidation.[10,36] In contrast, small oxide-free Zr metal particles (sub- to a few micrometers in diameter freshly produced from amorphous alloys by mechanical impact) can ignite at substantially lower temperature (about a few hundred degrees as shown in Sec. III. A) than Zr melting point (2128 K). This is attributed to their large surface-to-volume ratios, complete oxide-free surface states, and large surface strains on small particles lowering the oxygen diffusion barrier.

B. Oxygen concentration effect

In addition to the above-discussed microstructure, the combustion of metal fragments is strongly dependent on the oxygen concentration or partial pressure. Figure 8 plots several characteristics of metal combustion as a function of oxygen concentration: (a) induction times, (b) burn times, (c) burn rates, and (d) burst temperatures, all as a function of oxygen concentration. These experiments were performed on Zr-rich amorphous alloys under mechanical impacts in controlled O_2–N_2 gas mixtures with various O_2 concentrations from 5% to 100% by volume. At 5% O_2 content, very weak light emission is observed from high-speed camera. This level of light was registered only on two optical channels of the pyrometer with the voltage output less than 1 mV, which makes it difficult to determine the temperature. Therefore, it seems that 5% O_2 concentration is deemed as the combustion threshold at the present setup.

Note that the induction period decreases nonlinearly with the O_2 concentration [Fig. 8(a)] by about a few microseconds (or ~30%) over the entire concentration range. The burn time [Fig. 8(b)], on the other hand, increases linearly with the O_2 pressure, from 50 μs at 10% O_2 to 300 μs at 100% O_2, representing an extended level (or larger amount) of burning particles under the presence of sufficient O_2. These results are expected as higher O_2 concentration provides a larger driving force for oxygen diffusion and, thereby, a faster diffusion rate [Fig. 8(a)] and a longer diffusion distance [Fig. 8(b)]. The burn rate [Fig. 8(c)] increases with the O_2 content but slows down and rapidly reaches the maximum burn rate of 700×10^6 K/s above 50–60% O_2. As observed in Fig. 8(d), the burst temperature is largely independent of the O_2 concentration above 30%, below which it rapidly drops. Note that the burst temperature observed above 20–30% O_2 is about 500 K higher than that in air (~4000 K at ~21% O_2). The metal particle combustion is primarily controlled by two steps[1]: (i) the diffusion of oxidizer to the fuel source and (ii) the kinetics of the fuel oxidization. At low O_2 concentration (<30%), the dramatic decrease of peak temperature indicates that the availability of O_2 to the particles is the major constraint for the burning of metal particles, which is a diffusion-controlled process. Above 30% O_2 concentration, the leveling of the peak temperature implies that it is no longer bound by the oxygen diffusion but the heat balance in the combustion of metal particles.

Since the volatilization temperature of ZrO_2 (4280 K)[1] is below the boiling point of Zr metals (4703 K), the oxidation reaction of Zr metal is a heterogeneous surface process in condensed phase according to Glassman's criterion.[37] The volatilization temperature is the limit of maximum flame temperature possible because the energy for vaporization–dissociation of metal oxides is greater than the energy required to raise the metal oxides to their volatilization temperature. The burst temperature of

https://doi.org/10.1557/jmr.2012.302 Published online by Cambridge University Press

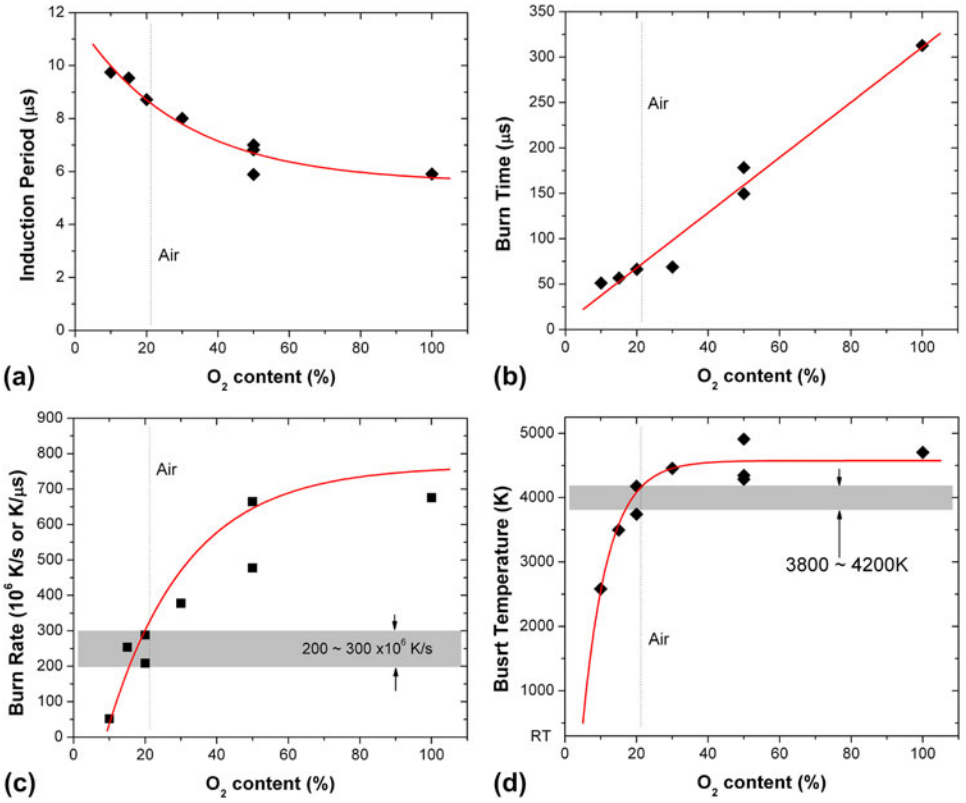


FIG. 8. The effect of oxygen content on the combustion kinetics of Zr-rich alloys. (a) Induction period, (b) burn time, (c) burn rate, and (d) burst temperature.

4000 K measured in air (or ~21% O_2) in the present study is then consistent with the Glassman's criterion. On the other hand, the burst temperature of about 4500 K measured above ~30% O_2 is higher than the volatilization temperature of ZrO_2. This may imply that some ZrO_2 particles are vaporized in high O_2 concentration, as we have often observed the explosion of small particles during combustion. Although the increased oxygen partial pressure can dramatically enhance the metal combustion, the reaction remains diffusion controlled because of the relatively large particle dimension (i.e., diffusion length). Such fact is evidenced by the linear increase of burn time with the oxygen content. This is different from the combustion of nanoparticles where the burning mechanism may switch to kinetically controlled process limited by the surface reaction rate because of the dramatically reduced oxygen diffusion length.

C. Thermal versus mechanical ignitions

The low ignition temperature observed under mechanical loadings in Fig. 3 indicates different combustion mechanisms between thermal (laser ablation) and mechanical (impact fracture) ignitions. The substantially lower ignition temperature than the Zr melting point (2128 K) thus initiates the reaction at a relatively slow rate with an extended induction period. As the reaction progresses, however, the temperature of metal fragments rapidly increases by the chemical energy from oxidation processes. On the other hand, the present pulse laser heating rapidly heats a small area of the metal strip above the Zr melting temperature, resulting in the ejection of small molten particles, where the reaction initiates and progresses very rapidly.

This difference in ignition temperature has dramatic impact on the combustion kinetics. Our previous measurements[13] on single particle combustion indicate that the burn time (t) of small particles follows a different power law dependence, $t \propto D^{1.5}$ for impact-initiated small particles versus $t \propto D^{1.8}$ for laser-initiated particles, both in the particle diameter range between 1 and 15 μm. As mentioned above, the higher ignition temperature in laser ablation dramatically shortens the incubation period and therefore greatly promotes the burning fast with a shorter burning period for laser ignition. As a result, a higher power dependence is observed.

Because of the low ignition temperature of fresh oxygen-free small particles produced from metallic glass under mechanical impacts, the ways how these particles release chemical energy depend strongly on microstructures and compositions of metallic glass. Figure 9(a), e.g., compares the time-resolved temperatures measured from two different Zr-rich amorphous alloys of with (red) and

https://doi.org/10.1557/jmr.2012.302 Published online by Cambridge University Press

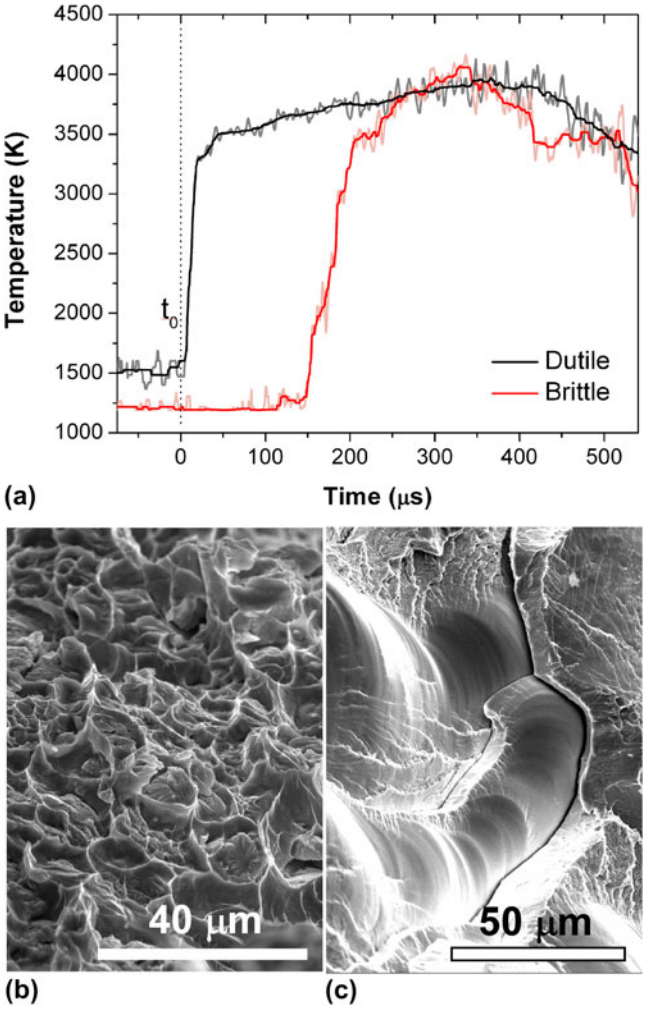


FIG. 9. (a) The time-resolved temperature evolution showing the influence of materials properties and microstructures on the induction period and burn rate of combustion. Comparison of fracture surface microstructures of ductile (b) and brittle (c) Zr-rich amorphous alloys under same mechanical impact conditions. Ductile alloys undergo considerably larger plastic deformation than brittle ones.

without (black) postheat treatment under the same impact velocity (~100 m/s). It is known that the heat treatment renders Zr-metallic glass more brittle due to the reduction of free volume.[38,39] As a result, significant differences are observed in the temperature profiles, both in the induction periods and burn rates. The untreated "ductile" alloy burns fast ($\sim 100 \times 10^6$ K/s—the slope of the rising edge) with nearly no induction period (less than a few microseonds), whereas the heat-treated brittle alloy burns relatively slow ($\sim 40 \times 10^6$ K/s) after a long induction period of ~150 μs.

These differences can be understood in terms of a larger amount of kinetic (impact) energy being absorbed in a more "ductile" material, converting it into thermal energy through mechanical deformation as evidenced by the scanning electron microscopy (SEM) characterization of the fracture surfaces of the two alloys as shown in Figs. 9(b) and 9(c). "Grass"-like pull-up features are observed on the fracture surface of the ductile alloy [Fig. 9(b)], which indicate significant plastic deformation and softening occur during the fracture. In contrast, relative smooth shale-like features are prevalent in the brittle alloy [Fig. 9(c)], implying dramatically less plastic flow. Consequently, the ductile alloy would convert a considerably larger amount of kinetic energy from the incident BB ball into thermal energy than the brittle alloy. This would increase the temperature of material and help to overcome the activation energy barrier in oxidation. Therefore, the induction period is greatly shortened, and combustion starts earlier and faster than a more brittle material. At relatively low impact velocity (<100 m/s), the crack propagation and opening become slower, during which the mechanical heat can be accumulated to initiate the combustion. The difference in the induction period, however, decreases as the impact velocity increases [see Fig. 5(c)] and eventually disappears at high velocities above ~150 m/s.

V. CONCLUSION

We presented our recent developments of time-resolved optical and x-ray diffraction methods, capable of probing dynamic responses of reactive metals under thermal and mechanical loadings. These include (i) high-speed microphotography to probe mechanical fragmentation and fragments combustion in microsecond time scales, (ii) multichannel optical pyrometry to measure nanosecond time-resolved temperatures from metal fragments in combustion, and (iii) time- and angle-resolved synchrotron x-ray diffraction to measure structural and chemical evolutions associated with metal combustions. These diagnostics enable us to determine chemical mechanisms and kinetics of reactive metals in various structures ranging from pure metallic foils to small (sub to 10 μm) metal particles produced by bulk metallic glass and nanometer-scale reactive multilayers.[19]

For quantitative description of combustion kinetics, we presented a combustion model based on the characteristics of time-resolved temperature profiles such as the induction period, burn time, burst temperature, and burn rate. The results showed strong dependences of combustion processes on (i) the exact nature of fragments including the particle size, distribution, as well as microstructures; (ii) chemical environment such as oxygen concentration; and (iii) thermal or mechanical ignition conditions.

The time- and angle-resolved synchrotron x-ray results indicated that a "simple" oxidation reaction of elemental metals like Zr is not so straightforward but undergoes a wide range of chemical and phase transformations. The results show that Zr combustion occurs heterogeneously on the surface, controlled by oxygen diffusion and solubility in metal matrix. The fundamental (atomistic) information regarding the structural and chemical evolution

https://doi.org/10.1557/jmr.2012.302 Published online by Cambridge University Press

associated with metal combustion is not only important to understand the observed chemical kinetics but also provides critical constraints for validating materials models often used to explain the large-scale integrated experimental results as well as timely and interactive information for tailoring materials characteristics (composition, microstructure, and geometry) for better mechanical and chemical performance.

ACKNOWLEDGMENTS

We appreciate Dr. Atakan Peker at Applied Science Laboratory at WSU, who provided Zr-rich bulk metallic glass used in the present study. We also recognize the contribution of Dr. Jing-Yin Chen at LLNL and Dr. Guoyin Shen at HPCAT/APS in time-resolved x-ray diffraction experiments. The x-ray work was done using the microdiffraction beamline (16IDD) at the High Pressure Collaborating Access Team (HPCAT) of the APS. Use of the HPCAT facility was supported by DOE-BES, DOE-NNSA (CDAC, LLNL, UNLV), NSF, DOD-TACOM, and the W.M. Keck Foundation. The present study has been supported by the DARPA (Grant No. W911NF-09-C-0033), U.S. DHS under Award Nos. 2008-ST-061-ED0001, DTRA (Grant No. HDTRA 1-09-1-0041), and NSF-DMR (Grant No. 0854618). The views and conclusions contained in this document are those of the authors and should not be interpreted as necessarily representing the official policies, either expressed or implied, of the U.S. Department of Homeland Security.

REFERENCES

1. R.A. Yetter, G.A. Risha, and S.F. Son: Metal particle combustion and nanotechnology. *Proc. Combust. Inst.* **32**, 1819 (2009).
2. D.D. Dlott: Thinking big (and small) about energetic materials. *Mater. Sci. Technol.* **22**, 463 (2006).
3. E.L. Dreizin: Metal-based reactive nanomaterials. *Prog. Energy Combust. Sci.* **35**, 141 (2009).
4. B.L. Holian: *Molecular Dynamics Simulations of Detonation Phenomena* (ITRI Press, McLean, VA, 2004).
5. K. Park, D. Lee, A. Rai, D. Mukherjee, and M.R. Zachariah: Size-resolved kinetic measurements of aluminum nanoparticle oxidation with single particle mass spectrometry. *J. Phys. Chem. B* **109**, 7290 (2005).
6. J.J. Granier and M.L. Pantoya: Laser ignition of nanocomposite thermites. *Combust. Flame* **138**, 373 (2004).
7. D. Skinner, D. Olson, and A. Block-Bolten: Electrostatic discharge ignition of energetic materials. *Propellants Explos. Pyrotech.* **23**, 34 (1998).
8. K.H. Ewald, U. Anselmi-Tamburini, and Z.A. Munir: Combustion of zirconium powders in oxygen. *Mater. Sci. Eng., A* **291**, 118 (2000).
9. R.J. Gill, C. Badiola, and E.L. Dreizin: Combustion times and emission profiles of micron-sized aluminum particles burning in different environments. *Combust. Flame* **157**, 2015 (2010).
10. M.A. Trunov, M. Schoenitz, and E.L. Dreizin: Ignition of aluminum powders under different experimental conditions. *Propellants Explos. Pyrotech.* **30**, 36 (2005).
11. Y. Huang, G.A. Risha, V. Yang, and R.A. Yetter: Effect of particle size on combustion of aluminum particle dust in air. *Combust. Flame* **156**, 5 (2009).
12. M.A. Trunov, M. Schoenitz, and E.L. Dreizin: Effect of polymorphic phase transformations in alumina layer on ignition of aluminium particles. *Combust. Theor. Model.* **10**, 603 (2006).
13. H. Wei and C-S. Yoo: Kinetics of small single particle combustion of zirconium alloy. *J. Appl. Phys.* **111**, 023506 (2012).
14. E.L. Dreizin: Effect of phase changes on metal-particle combustion processes. *Combust. Explo. Shock.* **39**, 681 (2003).
15. M.A. Trunov, M. Schoenitz, X.Y. Zhu, and E.L. Dreizin: Effect of polymorphic phase transformations in Al_2O_3 film on oxidation kinetics of aluminum powders. *Combust. Flame* **140**, 310 (2005).
16. E.L. Dreizin: Phase changes in metal combustion. *Prog. Energy Combust. Sci.* **26**, 57 (2000).
17. I.E. Molodetsky, E.L. Dreizin, and C.K. Law: Evolution of particle temperature and internal composition for zirconium burning in air. *Proc. Combust. Inst.* **26**, 1919 (1996).
18. H. Wei and C.S. Yoo: Dynamic structural and chemical responses of energetic solids. in *Advances in Energetic Materials Research*, edited by M.R. Manaa, C.-S. Yoo, E.J. Reed, and M.S. Strano (Mater. Res. Soc. Symp. Proc. **1405**, Warrendale, PA, 2012). mrsf11-1405-y02-01.
19. C.S. Yoo, H. Wei, J.-Y. Chen, G. Shen, P. Chow, and Y. Xiao: Time- and angle-resolved x-ray diffraction to probe structural and chemical evolution during Al-Ni intermetallic reactions. *Rev. Sci. Instrum.* **82**, 113901 (2011).
20. J.C. Trenkle, L.J. Koerner, M.W. Tate, S.M. Gruner, T.P. Weihs, and T.C. Hufnagel: Phase transformations during rapid heating of Al/Ni multilayer foils. *Appl. Phys. Lett.* **93**, 081903 (2008).
21. J.C. Trenkle, L.J. Koerner, M.W. Tate, N. Walker, S.M. Gruner, T.P. Weihs, and T.C. Hufnagel: Time-resolved x-ray microdiffraction studies of phase transformations during rapidly propagating reactions in Al/Ni and Zr/Ni multilayer foils. *J. Appl. Phys.* **107**, 113511 (2010).
22. H. Wei, C.-S. Yoo, J.-Y. Chen, and G. Shen: Oxygen-diffusion limited metal combustions in Zr, Ti, and Fe foils: Time- and angle-resolved x-ray diffraction studies. *J. Appl. Phys.* **111**, 063528 (2012).
23. K. Fadenberger, I.E. Gunduz, C. Tsotsos, M. Kokonou, S. Gravani, S. Brandstetter, A. Bergamaschi, B. Schmitt, P.H. Mayrhofer, C.C. Doumanidis, and C. Rebholz: In situ observation of rapid reactions in nanoscale Ni-Al multilayer foils using synchrotron radiation. *Appl. Phys. Lett.* **97**, 144101 (2010).
24. W.M. Haynes: *CRC Handbook of Chemistry and Physics*, 92nd ed. (CRC Press, Boca Raton, FL, 2011).
25. W.H. Jiang, F.X. Liu, H.H. Liao, H. Choo, P.K. Liaw, B.J. Edwards, and B. Khomami: Temperature increases caused by shear banding in as-cast and relaxed Zr-based bulk metallic glasses under compression. *J. Mater. Res.* **23**, 2967 (2008).
26. H.A. Bruck, A.J. Rosakis, and W.L. Johnson: The dynamic compressive behavior of beryllium bearing bulk metallic glasses. *J. Mater. Res.* **11**, 503 (1996).
27. C.J. Gilbert, J.W. Ager, V. Schroeder, R.O. Ritchie, J.P. Lloyd, and J.R. Graham: Light emission during fracture of a Zr-Ti-Ni-Cu-Be bulk metallic glass. *Appl. Phys. Lett.* **74**, 3809 (1999).
28. S.E. Olsen and M.W. Beckstead: Burn time measurements of single aluminum particles in steam and CO_2 mixtures. *J. Propul. Power* **12**, 662 (1996).
29. E.L. Dreizin: On the mechanism of asymmetric aluminum particle combustion. *Combust. Flame* **117**, 841 (1999).
30. S. Rossi, E.L. Dreizin, and C.K. Law: Combustion of aluminum particles in carbon dioxide. *Combust. Sci. Technol.* **164**, 209 (2001).
31. H. Wei and C.S. Yoo: in preparation.
32. D. Kovalev, V. Shkiro, and V. Ponomarev: Dynamics of phase formation during combustion of Zr and Hf in air. *Int. J. Self Propag. High Temp. Synth.* **16**, 169 (2007).
33. ASM Alloy Phase Diagrams Center: Diagram No. 103569, 101191.

https://doi.org/10.1557/jmr.2012.302 Published online by Cambridge University Press

34. T. Arai and M. Hirabayashi: Oxygen ordering in the Zr-O alloy: A structural, calorimetric and resistometric study. *J. Less-Common Met.* **44**, 291 (1976).
35. R. Arroyave, L. Kaufman, and T.W. Eagar: Thermodynamic modeling of the Zr-O system. *Calphad* **26**, 95 (2002).
36. I.G. Assovskiy, V.I. Kolesnikov-Svinarev, G.P. Kuzhnetsov, and O.M. Zhigalina: Gravity effect in aluminum droplet ignition and combustion. In *5th International Microgravity Combustion Workshop, Cleveland, OH, 1999*. Proceedings of the Fifth International Microgravity Combustion Workshop, NASA, May 18–20, 1999, Cleveland, OH; pp. 223–226.
37. I. Glassman: *Combustion*, 3rd ed. (Academic Press, Inc., San Diego, CA, 1996).
38. W.F. Wu, Z. Han, and Y. Li: Size-dependent "malleable-to-brittle" transition in a bulk metallic glass. *Appl. Phys. Lett.* **93**, 061908 (2008).
39. P. Murali and U. Ramamurty: Embrittlement of a bulk metallic glass due to sub-Tg annealing. *Acta Mater.* **53**, 1467 (2005).

https://doi.org/10.1557/jmr.2012.302 Published online by Cambridge University Press